Journal of Materials Processing Tech. 299 (2022) 117329

Contents lists available at ScienceDirect

Journal of Materials Processing Tech.

journal homepage: www.elsevier.com/locate/jmatprotec

Improvement of penetration ability of heat source for 316 stainless steel welds produced by alternating magnetic field assisted laser-MIG hybrid welding

Fuyun Liu [a], Bingxiao Xu [a], Kuijing Song [b,*], Caiwang Tan [a,*], Hongyun Zhao [a], Guodong Wang [a], Bo Chen [a], Xiaoguo Song [a]

[a] State Key Laboratory of Advanced Welding and Joining, Harbin Institute of Technology, Harbin, 150001, China
[b] School of Materials Science and Engineering, Hefei University of Technology, Hefei, 230009, China

ARTICLE INFO

Associate Editor: S-J. Na

Keywords:
Penetration ability
Alternating magnetic field
Laser-MIG hybrid welding
Welding plasmas
Droplet transition
Keyhole behavior

ABSTRACT

An alternating magnetic field was designed to increase weld depth of laser-MIG hybrid welded 316 stainless steel joint. The influencing mechanism of alternating magnetic field on improving penetration ability of hybrid heat source of laser-MIG hybrid welding was revealed. The results suggested that the difference of weld depth under different magnetic flux density was attributed to the change of characteristics of arc plasma and laser-induced plasma, droplet transition and keyhole behavior. More compressed arc shape under lower magnetic flux density (LMFD) with 20 m T and 30 m T promoted laser-induced plasma to move along the channel of laser beam, leading to decrease of weld depth. However, the laser-induced plasmas could be dispersed away from the channel of laser beam under higher magnetic flux density (HMFD) of 60 m T and 90 m T, which was the main reason for the increased penetration ability of hybrid heat source. Besides, the droplet transferred to behind the keyhole instead of dropping into the keyhole and more stable keyhole was obtained under HMFD, which were also beneficial for deeper penetration depth of laser energy. Moreover, the motion behavior of charged particles of arc plasma and laser-induced plasma and forces condition of droplet transition were discussed in magnetic field assisted laser-MIG hybrid welding.

1. Introduction

Recently, laser-arc hybrid welding technology combining both heat sources of laser and arc has attracted widespread attentions, due to its unique advantages, as stated by (Steen William, 1980). (Bagger and Olsen, 2005) also reported that compared to single laser welding or arc welding, laser-arc hybrid welding possessed better gap bridging, faster welding speed and higher penetration depth, benefiting from the strong laser-arc synergistic effects. However, (Dilthey and Wieschemann, 1999) pointed out that the coupling process of laser beam and arc was complicated when considering the interaction between heat sources and base material during laser-arc hybrid welding. Droplet transition, characteristics of arc plasma and laser-induced plasma, melt flowing and keyhole behaviors are included in laser-MIG hybrid welding process. Meanwhile, these characteristics have significant influences on quality of laser-MIG hybrid welded joint.

The weld depth, as a main characteristic of weld quality, has always been the focus of attention by relevant scholars. For laser-arc hybrid welding method, the weld depth was mainly determined by laser heat source, due to stronger penetration ability of laser energy. The relevant studies about the penetration ability of single laser welding method have been performed and the mechanism of laser-induced plasma plume on laser penetration ability has been clarified. (Chiang and Aibright, 1992) found that the heat transfer efficiencies in laser beam welding could be suppressed by lase-induced plasma plume during CO2 laser welding of mild steel. (Zuo et al., 1998) also pointed out that laser-induced plasma could shield incident laser beam and about 50 % incident laser energy would be absorbed when plasma shielding occurred during high power CO2 laser materials processing. (Kawahito et al., 2009) studied the attenuation effect of plasma plume on near-infrared laser beam and suggested that the attenuation of laser energy was about 3 %–13 % during laser welding by probe laser beam measurements, and similar results have also been found by (Shcheglov et al., 2011). Besides, (Gao et al., 2015) studied the characteristics of laser-induced plasma plume

* Corresponding authors.
E-mail addresses: songkuijing@hfut.edu.cn (K. Song), tancaiwang@hitwh.edu.cn (C. Tan).

https://doi.org/10.1016/j.jmatprotec.2021.117329
Received 10 April 2021; Received in revised form 18 July 2021; Accepted 13 August 2021
Available online 16 August 2021

during fiber laser welding aluminum alloy and found that the laser beam energy was attenuated by plasma plume in laser beam path by absorption, refraction and scattering. The shielding effect was dominated by the inverse bremsstrahlung effect of plasma. Based on above studies, to decrease the shielding effect of plasma plume on laser energy and improve penetration depth, various methods including side-assisted gas and application of vacuum or subatmospheric pressure were employed in laser welding process, as discussed by (Katayama et al., 2011) and (Luo et al., 2015). However, these methods were not suitable for laser-arc hybrid welding to reduce the negative effect of laser-induced plasma plume, due to the existence of arc plasma. In addition, (Üstündağ et al., 2021) has proposed that the keyhole stability was also an important factor influencing the penetration ability of laser beam because part of laser energy was lost for maintaining the stability of keyhole. Compared to single laser welding, the melt flow was more complicated and the keyhole was more fluctuant during laser-MIG hybrid welding, due to the impact of the force by droplet transfer. With the expectation for expanding application of laser-MIG hybrid welding, it was necessary to seek an auxiliary method to improve penetration depth of laser-MIG hybrid welding under the premise of ensuring quality of welded joint.

In the past decades, magnetic field assisted welding technology has been employed in traditional arc welding or laser welding. The significant importance of the magnetic field on arc behaviors, droplet transition, laser-induced plasma and melt flow has been studied. (Wang et al., 2017) suggested the external magnetic field could control the shape and movement of arc plasma by adjusting direction and parameters of magnetic field. (Bachmann et al., 2016) employed a steady magnetic field in laser welding process and found that the Hartmann effect produced by external magnetic field could affect the flow dynamics of melt in the molten pool. As (Tse et al., 1999) reported, the laser-induced plasma could be controlled by external magnetic field, leading to 7 % increase of the penetration depth during CO2 laser welding. (Li et al., 2018) claimed that the stabilization of keyhole could be improved by external magnetic field during laser full penetration welding. Moreover, (Üstündağ et al., 2021) studied the effect of an oscillating magnetic field on the keyhole stability and found that a direct influence of external magnetic forces on the flows in the keyhole surrounding was beneficial for keyhole stabilization. The aforementioned studies confirmed that the application of the external magnetic field had a significant influence on arc welding and laser welding process. However, the researches about effect of external magnetic field on penetration ability of laser-MIG hybrid welding were not carried out. The complicated interaction mechanism between magnetic field and characteristics of laser-MIG hybrid welding process should also be clarified.

Therefore, in this study, in order to explore the effect of external magnetic field on penetration ability of hybrid heat sources during laser-MIG hybrid welding, laser-MIG hybrid welding at various alternating magnetic flux density was performed. The characteristics of hybrid plasmas including arc plasma and laser-induced plasma under different magnetic flux density were monitored and the droplet transition and the dynamic behavior of the keyholes were observed through a “sandwich” test method. Moreover, the penetration mechanism of hybrid heat source to welded plate under alternating magnetic field was detailly studied.

2. Experimental procedure

2.1. Materials and welding setup

In this study, the 316 stainless steel plates with the dimension of 150 mm × 100 mm × 6 mm and the ER316 L filler wire with diameter of 1.2 mm were employed as welding materials. The chemical compositions of 316 stainless steel and ER316 L filler metal were listed in Table 1. Before welding, the 316 stainless steel plates were cleaned by alcohol to remove away the grease. The pure argon was employed as shielding gas to protect the molten pool.

A fiber laser system (IPG YLS-6000) coupled with an arc welding system (Lincoln Power Wave R350) and KUKA welding robot was used in the experiment. The wavelength, laser focal length and BPP of laser beam were 1.06 μm, 300 mm and 6 mm·mrad., respectively, and the range of arc current was from 50 A to 280 A. Besides, alternating magnetic field with sine waveform was generated by a special magnet system and the maximum magnetic flux density reached to 200 m T.

2.2. Welding process parameters

The bead-on-plate welding was performed by the laser-MIG hybrid welding process. Fig. 1(a) showed the experimental process of laser-MIG hybrid welding under the alternating magnetic field. The laser beam was deviated 10°from the Z axis to protect the optical component from possible damage. The magnetic coil was placed directly below the laser beam and base metal. The laser head, arc torch and magnetic coil were fixed, while the work piece plate was driven to move in a direction. As shown in Fig. 1(b), the special magnet system included the power module, waveform generator, power amplifier and magnetic coil. The power module was employed to supply power for waveform generator and then electric current with sine waveform was transferred to the power amplifier. The alternating magnetic field with sine waveform would be generated when amplified electric current with sine waveform passed through the winding magnetic coil. After preliminary trials, the constant processing parameters were set as follows: laser power was 3500 W, welding current was 180 A, welding voltage was 21 V, welding speed was 1.0 m/min, wire feed speed was 7.5 m/min, distance between the laser and arc was 3 mm, laser defocusing distance was 0 mm, shielding gas flow rate was 20 L/min. Additionally, the magnetic flux density was measured by a high precision gauss meter before welding and the measurement position was located below the base plate and above the center of magnetic coil. The magnetic flux density from 0 m T to 90 m T was considered as the main variation while the frequency was set as a constant of 1000 Hz during the welding process.

2.3. Monitoring of welding process

Fig. 2 depicted the monitoring schematic of laser-MIG hybrid welding process under the alternating magnetic field. As shown in Fig. 2 (a), morphology of arc plasma and laser-induced plasma were directly monitored by the high-speed video camera (i-SPEED 221). The characteristics of hybrid welding plasmas were obtained by an AvaSpec-ULS2048−8-USB2 spectrograph and the electron density of plasmas was estimated from the spectrum data by using Stark broadening effect. As depicted in Fig. 2 (b), a “sandwich” method was employed to obtain droplet transitions and keyhole behaviors inside the molten pool. The droplet transitions and keyhole behaviors were observed by the camera with an ultraviolet (UV) filter of 550 nm and optical filter of ND 8 lenses.

Table 1
Chemical compositions of 316 stainless steel and ER316 L (wt.%).

Element	C	Mn	P	Si	Cr	Ni	Mo	Fe
316	≤0.08	≤2.0	≤0.045	≤1.0	16–18	10–14	2–3	Bal.
ER316L	0.02	1.85	0.009	0.38	18.73	12.5	2.21	Bal.

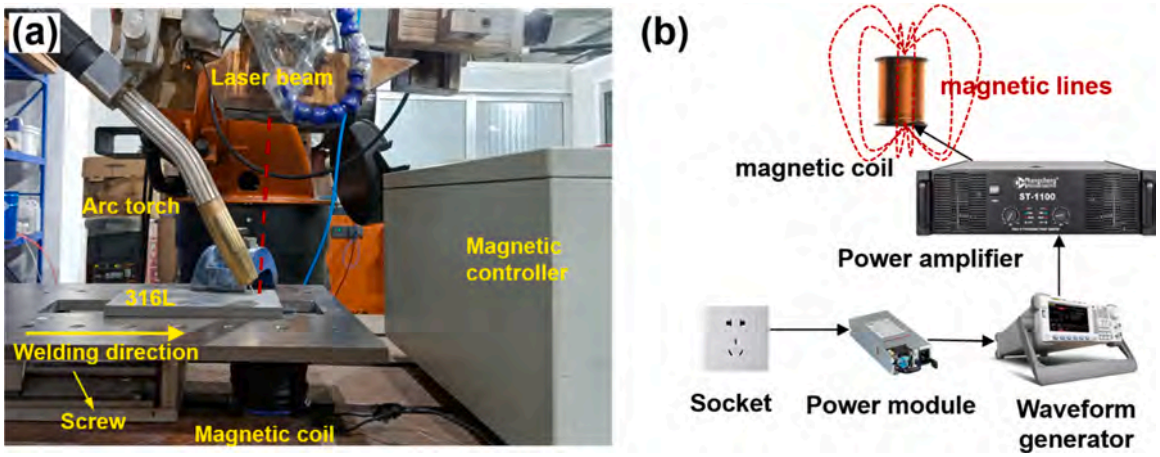

Fig. 1. (a) Schematic of laser-MIG hybrid welding process assisted by alternating magnetic field; (b) configuration of the external magnetic field.

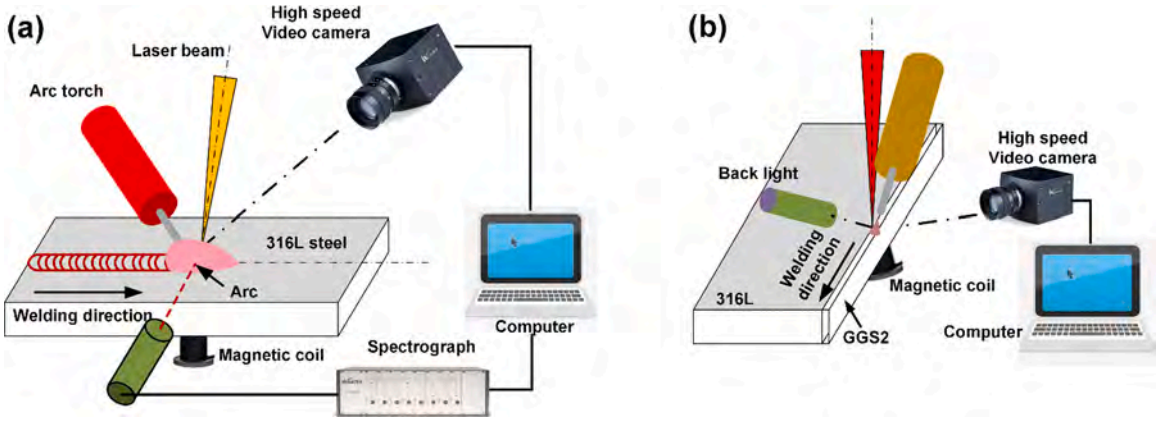

Fig. 2. Monitoring schematic of laser-MIG hybrid welding under alternating magnetic field: (a) acquisition of welding plasmas; (b) the "sandwich" method.

3. Results and discussion

3.1. Appearance and cross-sectional morphology

The laser-MIG hybrid welding tests under each magnetic flux density were performed at least three times to ensure the reliability of the experimental results. The typical appearance and cross-sectional morphology of 316 stainless steel laser-MIG hybrid welded joints under different magnetic flux density were shown in Fig. 3. In addition, the average values of weld cross-sectional features including weld depth, weld width and depth to width obtained under different magnetic flux density from multiple tests were calculated. The corresponding statistics of depth and width to depth versus magnetic flux density were depicted in Fig. 4. As shown in Fig. 3, with the increasing magnetic flux density, the more and more tortuous weld bead was obtained and slightly more instable laser-MIG hybrid welding process was observed, which suggested that external alternating magnetic field had an effect on laser-MIG hybrid welding process. Besides, the depth and depth to width of welds were 4.08 ± 0.06 mm and 0.709 ± 0.005, respectively, without an alternating magnetic field. The magnetic flux density was divided into low- and high-magnetic flux density with the threshold of 40 m T. The significant difference of the low and high magnetic flux density on weld depth was clearly identified. When low magnetic flux density (B = 20 m T & B = 30 m T) was employed, the weld depth and depth to width were 3.14 ± 0.08 mm, 3.96 ± 0.12 mm and 0.503 ± 0.008, 0.617 ± 0.025, respectively, which were less than that when B = 0 m T. However, when high magnetic flux density (B = 40 m T, B = 60 m T and B = 90mT) were used, larger weld depths (4.17 ± 0.03 mm, 4.24 ± 0.08 mm and 4.35 ± 0.09 mm) were observed compared to that without a magnetic flux density. Besides, the depth to width reached to maximum value (0.77 ± 0.004) when B = 40 m T, while depth to width of welds (0.69 ± 0.001 and 0.70 ± 0.006) when B = 60 m T and B = 90 m T were slightly lower than that (0.709 ± 0.005) when B = 0 m T. The weld depth was determined by the penetration ability of laser-MIG hybrid heat source to welded plate. Therefore, alternating magnetic field exerted a significant effect on penetration ability of hybrid heat source and the effect was related with the magnetic flux density.

3.2. Affecting mechanism of AMF on penetration ability

3.2.1. Characteristics of hybrid welding plasmas under AMF

For the laser-MIG hybrid welding method, the depth of weld was mainly dependent on laser energy. During the laser penetration welding, the keyhole was formed inside the molten pool due to interaction between high-energy laser beam and base materials. Meanwhile, the metal vapor evaporated from keyhole wall was ionized and the laser-induced plasma was generated inside the keyhole. Subsequently, the charged particles of laser-induced plasma from the keyhole was erupted and mixed with charged particles of the arc plasma when charged particles of laser-induced plasma passed through the zone of arc plasma. Finally, these charged particles gradually disappeared in the upper of arc zone with the decrease of temperature. (Tse et al., 1999) pointed out that the

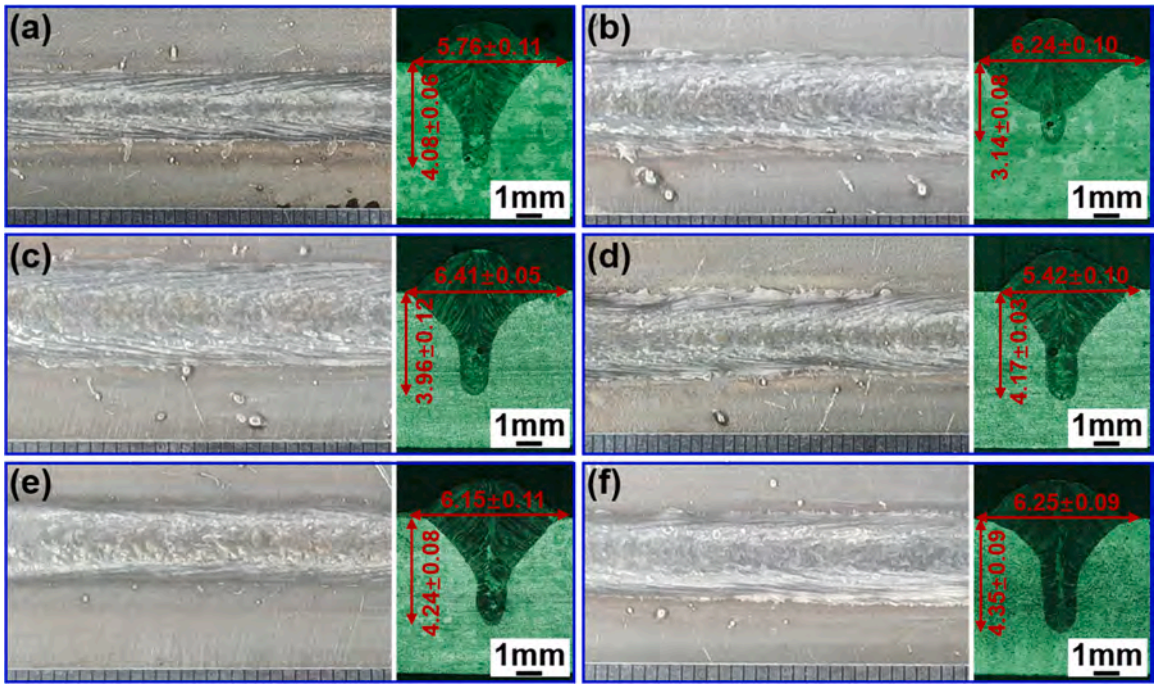

Fig. 3. Appearance and cross-sectional morphology of 316 stainless steel hybrid welded joints under different magnetic flux density: (a) B = 0 m T; (b) B = 20 m T; (c) B = 30 m T; (d) B = 40 m T; (c) B = 60 m T; (d) B = 90 m T.

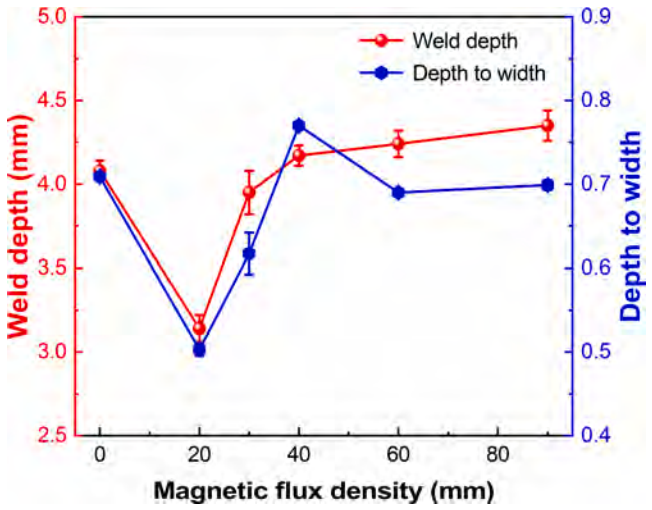

Fig. 4. Depth and depth to width of the weld under different magnetic flux density.

laser-induced plasma in the channel of the laser beam could significantly reduce the energy of laser beam by scattering and absorbing laser energy, namely shielding effect of plasma, which was also expounded by (Wang et al., 2011) and (Chen et al., 2019).

Figs. 5 and 6 showed morphology of arc plasma and laser-induced plasma plume in a period during laser-MIG hybrid welding of 316 stainless steel under different magnetic flux density. As shown in Fig. 5, when no magnetic flux density (NMFD) was employed, at t_0+5 ms - t_0+10 ms, the obvious laser-induced plasma plume was ejected from keyhole and passed through the arc zone. Bright laser-induced plasma plume was observed at the channel of the laser beam, implying a strong shielding effect. When magnetic flux density increased to 20 m T and 30 m T, larger volume and longer time of laser-induced plasma plumes were found at the channel of the laser beam in per period compared to that when B = 0 m T. However, as shown in Fig. 6, when magnetic flux density increased to 40 m T, volume of arc was more compressed in the whole period and part of the laser-induced plasma plumes appeared at one side away from the channel of the laser beam during t_0+3.0 ms - t_0+8.0 ms. With magnetic flux density further increasing to 60 m T and 90 m T, the shape of arc was further compressed and larger volume of the laser-induced plasma plume were dispersed away from channel of the laser beam. The above results verified the assumption that the external alternating magnetic field had a significant influence on the charged particles in the arc plasma and laser-induced plasma.

In order to further reveal the affecting mechanism of alternating magnetic field on penetration ability of hybrid heat source to welded plate, the electron density of plasma plume at the channel of laser beam was characterized by the method of spectral acquisition and analysis. Fig. 7 suggested the acquisition position and spectral line collected by spectral diagnosis. The acquisition location of spectral diagnosis was located 5 mm above the keyhole. As revealed in Fig. 7 (b), the spectral lines emitting from acquisition position at the channel of laser beam were composed of Fe I line and Ar I line, suggesting that two types of plasmas including more metal plasmas and part of arc plasmas were appeared in the channel of laser beam. In this work, the shielding effect of laser-induced plasma and arc plasma on laser energy was considered together.

Fig. 8 presented time-domain diagram of electron density obtained during laser-MIG hybrid welding under varying magnetic flux density. The average electron density versus magnetic flux density was shown in Fig. 9. The average electron density was firstly increased to the maximum when B = 20 m T and then decreased. When magnetic flux density was 0 m T, the electron density of hybrid plasmas in the acquisition position was $1.46 \times 10^{17}/cm^3$. With the magnetic flux density increasing to 20 m T and 30 m T, the average electron density increased to $1.55 \times 10^{17}/cm^3$ and $1.48 \times 10^{17}/cm^3$, respectively. However, when magnetic flux density increased from 40 m T to 90 m T, the average electron density reduced from $1.44 \times 10^{17}/cm^3$ to $1.38 \times 10^{17}/cm^3$. The above results suggested that the average electron density under LMFD was obviously higher, while the average electron density under HMFD was lower compared to that under B = 0 m T, which corresponded to the volume and brightness of laser-induced plasma

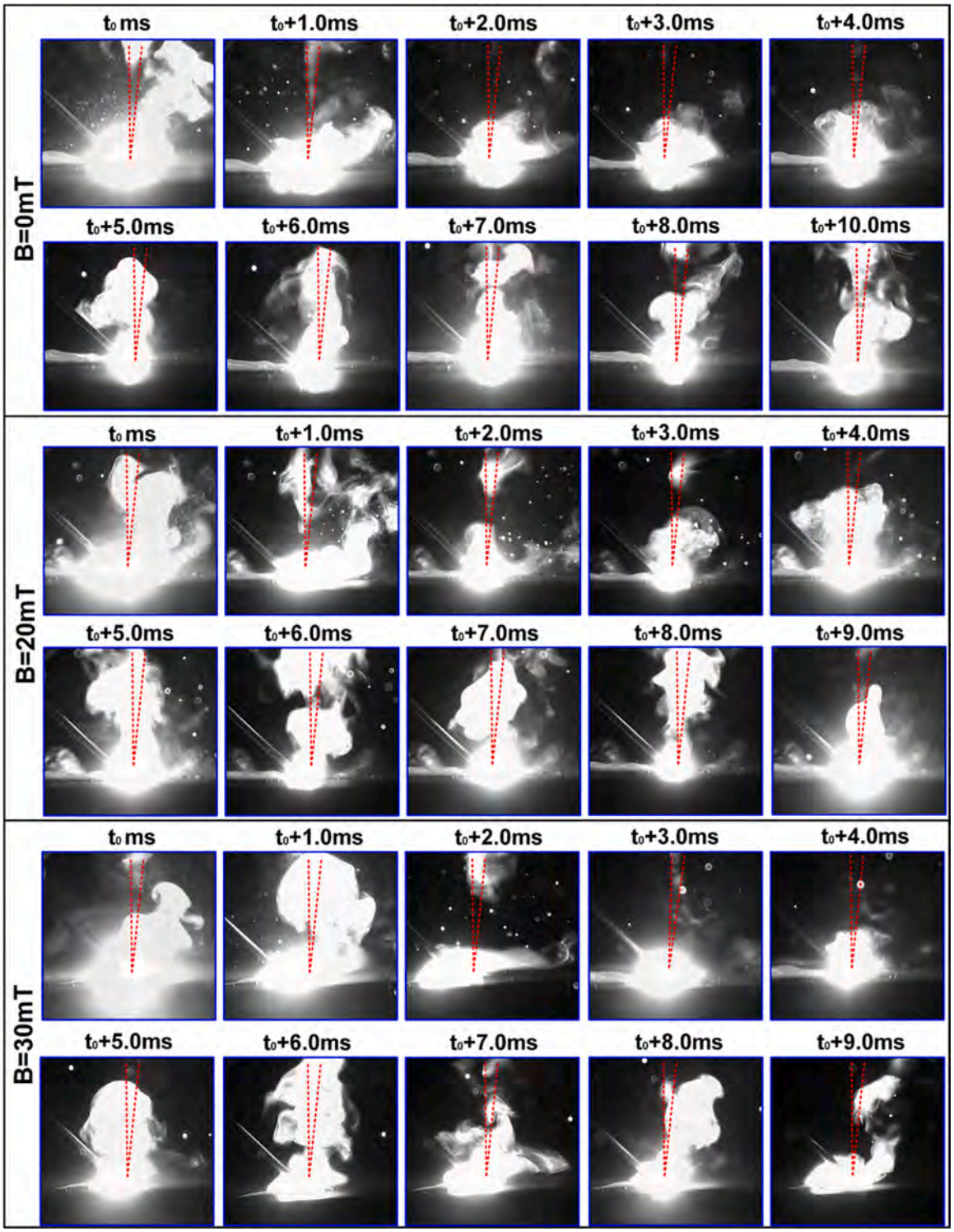

Fig. 5. Morphology of arc and metal plasma plume in a period during laser-MIG hybrid welding when B = 0 m T, B = 20 m T and 30 m T.

plume in the channel of laser beam presented in Figs. 5 and 6.

The motion of charged particles of arc plasma was mainly determined by arc blow force (***Fa***), the electric-field force (***Fe***) and self-induced magnetic-field force (***Fb***) during laser-MIG hybrid welding without a magnetic field. The arc blow force was generated due to the outflow of shielding gas from the nozzle, whose direction was from the nozzle to base metal. The arc flow force ***Fa*** could be calculated as

$$\boldsymbol{Fa} = \frac{1}{2} C_{ps} \rho_g v_g^2 \pi r_p^2 = 2 C_{ps} \rho_g \frac{Q^2}{\pi \left(R_n^2 - R_w^2\right)^2} r_p^2 \tag{1}$$

Where, C_{ps} was the drag coefficient for the sphere of ionized particle, ρ_g was the shielding gas density, v_g was the shielding gas velocity, r_p was the radius of ionized particle, Q was the inflow rate of the shielding gas, R_n and R_w were the radii of the gas nozzle and filler wire, respectively.

The high electric voltage was produced between wire tip (the positive pole) and base metal (the negative pole) during welding process. In

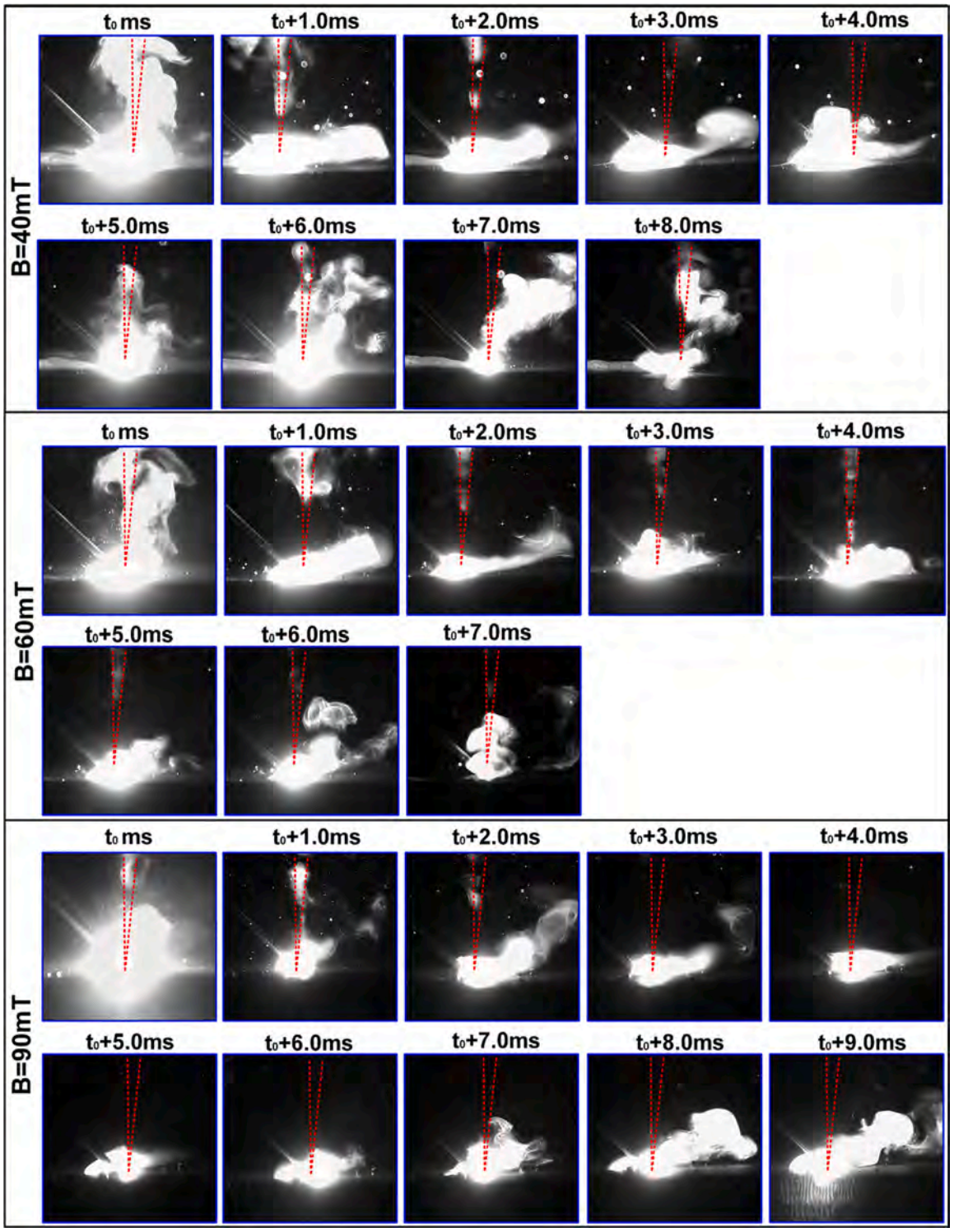

Fig. 6. Morphology of arc and metal plasma plume in a period during laser-MIG hybrid welding when B = 40 m T, B = 60 m T and B = 90 m T.

this case, the electric-field force would be generated when ionized particle was moving between wire tip and base metal. The electric-field force (***Fe***) could be represented as

$$\boldsymbol{Fe} = eE = e\frac{U}{D} = e\frac{IR}{D} = e\frac{I}{\sigma A} \tag{2}$$

Where, e was the charge of charged particle, E was the electric field intensity, U was the electric voltage from wire tip to base metal, D was the distance from wire tip to base metal, R was the electric resistance, σ was electric conductivity and A was cross section of the arc.

According to electromagnetic induction principle, the magnetic field would be generated by the electric field, namely self-induced magnetic field. The direction of the self-induced magnetic lines was clockwise along the axis direction of the electric field lines. The self-induced electromagnetic force ***Fb*** could be considered as

$$\boldsymbol{Fb} = \frac{\mu_0 I^2}{4\pi}\left\{ln\frac{r_p sin\theta}{r_w} - \frac{1}{4} - \frac{1}{1-cos\theta} + \frac{2}{(1-cos\theta)^2} ln\frac{2}{1+cos\theta}\right\} \tag{3}$$

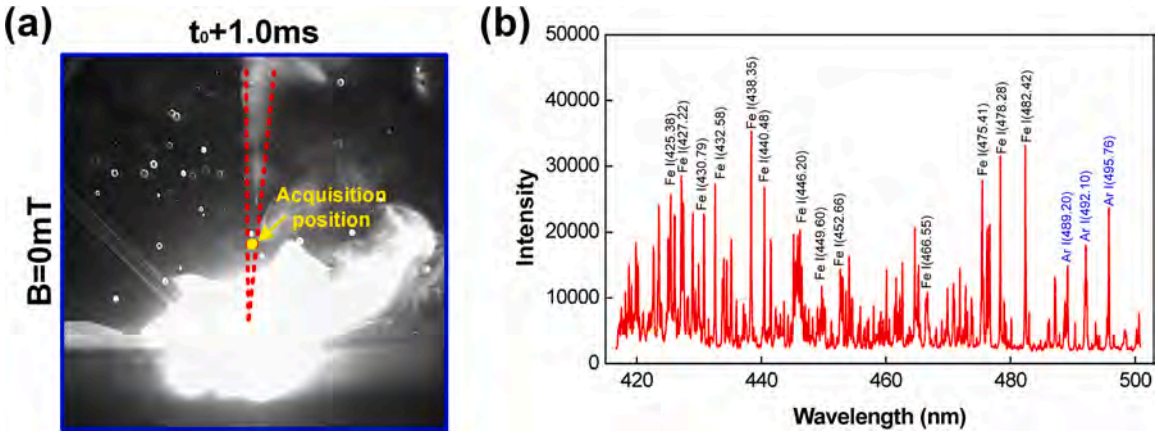

Fig. 7. The acquisition position and spectral line collected by spectral diagnosis. (a) acquisition position; (b) spectral line.

Where, I was the welding current, r_w was the radius of filler wire, respectively. θ was the maximum angle between the electrode axis and location of ionized particle.

As shown in Fig. 10 (a), the direction of electric field (E) inside the arc plasma was from wire tip (the positive pole) to weld pool (the negative pole). Therefore, the charged particles of arc plasma would move along the direct from wire tip (the positive pole) to weld pool (the negative pole) under the effect of arc blow force and electric-field force. Besides, the direction of magnetic field force was perpendicular to the motion direction of charged particles, as introduced by (Chen et al., 2012). According to Fleming's left-hand rule, the charged particles were driven toward the axis of filler wire under the self-induced magnetic field force (***Fb***). In this case, the more charged particles above filler wire was driven to move downward. Therefore, the motion direction of charged particles inside arc plasma was moving downward and away from wire tip under the effect of these forces, leading to compressed shape of arc. Besides, shape of arc plasma was also related with mixing of charged particles from laser-induced plasma. When charged particles of laser-induced plasma were ejected from keyhole and entered arc plasma, the charged particles in arc plasma would be increased during the laser-MIG hybrid welding. As a result, the ionizability of arc would be improved and the arc resistance would be reduced, which was consistent with the study of (Lacroix et al., 1997). According to the minimum voltage principle, the shape of arc would be further compressed, due to increasement of welding current, as reported by (Liu et al., 2017).

However, the shape of arc would be more compressed when external alternating magnetic field was employed in the laser-MIG hybrid welding. The Lorentz force could be produced by the interaction between the external alternating magnetic field and the charged particles that moved downwards and away from axis direct of wire line. The distribution of external magnetic field lines inside arc zone was depicted as the red dashed lines with arrow (Fig. 10 (b)). According to Fleming's left-hand rule, the Lorentz force (***FB***) produced by external magnetic field would be generated and the direction of Lorentz force (***FB***) exerted by charged particles in arc plasma was rotating downward around the axis of wire line. As a result, more compressed shape of arc plasma was observed under MFD compared to that without a magnetic field. Additionally, the direction of rotation was changed with the conversion of the external induced magnetic pole, and the magnitude of rotation force was constantly increased with increasing magnetic flux density. Therefore, the swing of arc appeared when HMFD was used.

The charged particles of laser-induced plasma were also affected by the external magnetic field. As shown in Fig. 10(c), the ionized particles ejected from keyhole tended to rapidly move along the channel of laser beam, due to strong force of metal vapor reaction (***Fv***). However, when ionized particles of laser-induced plasma passed through the arc zone, the particles of laser-induced plasma would be prevented from erupting along the laser beam channel, due to the effect of various forces. These forces were mainly composed of electric-field force (***Fe***) and self-induced magnetic field force (***Fb***). As presented in Fig. 10(c), the direction of electric-field force (***Fe***) and self-induced magnetic field force (***Fb***) exerted on the particles of laser-induced plasma were along axis direction of wire and away from laser beam, respectively.

As suggested in Fig. 10(d), "F_B" represented the Lorentz force of ionized particles of laser plasma produced by the external magnetic field, which had a positive effect on dispersing these ionized particles away from laser beam. In order to clearly analyze dispersing effect of external magnetic field on laser-induced plasma, a simplified model was established. As presented in Fig. 10(e), for the ionized particles moving along channel of laser beam, no external Lorentz force was applied on the ionized particle (#0) located in centerline of laser beam, because its motion direction was parallel with external magnetic line. However, the motion of ionized particles (#1 and #2) in the channel of laser beam would be affected by external Lorentz force. From the front view, the motion direction of ionized particles along channel of laser beam was perpendicular to the horizontal component of the external magnetic field (B_1). At the moment, the external Lorentz force (F_{B1}) would be generated and the motion direction of ionized particles would be changed. The velocity vector (V_{B1}) of ionized particles was perpendicular to the vertical component of the external magnetic field (B2), which led to generation of the other external Lorentz force (F_{B2}). Therefore, when HMFD was employed, strong external Lorentz force would change motion direction of ionized particles toward away from channel of laser beam, showing strong dispersing effect on laser plasma.

Therefore, arc plasma was more compressed as LMFD was used, which was beneficial for the laser-induced plasma to pass through arc plasma and move along the laser beam channel, due to shorter distance in vertical direction of arc plasma. Besides, the dispersing effect of external magnetic field on laser-induced plasma was lower under LMFD. In this case, stronger shielding effect on laser energy was generated under LMFD, leading to decrease of weld depth. However, when HMFD was employed, stronger dispersing effect produced by HMFD was much larger than the effect caused by compressed arc. As a result, the laser-induced plasma was dispersed away from the channel of laser beam under HMFD, showing weaker shielding effect on laser energy.

3.2.2. *Droplet transition and keyhole behavior under AMF*

Fig. 11 showed the dynamic behavior of the keyhole and the droplet transition during laser-MIG hybrid welding when magnetic flux density was 0 m T, 20 m T and 90 m T. During the laser-MIG hybrid welding process without an external magnetic field, the keyhole fluctuation

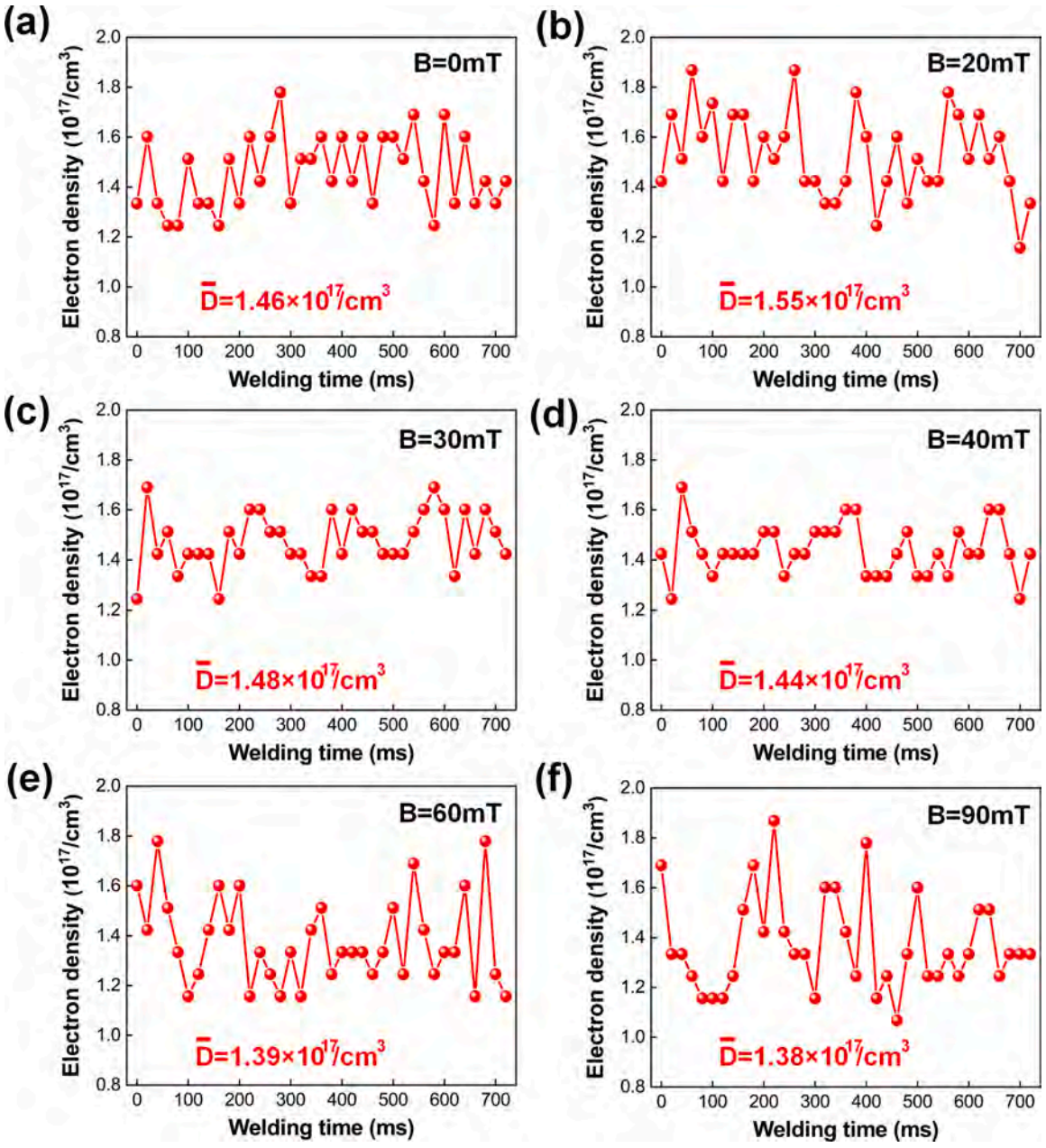

Fig. 8. The time-domain diagram of electron density during laser-MIG hybrid welding under the varying magnetic flux density: (a) B = 0 m T; (b) B = 20 m T; (c) B = 30 m T; (d) B = 40 m T; (e) B = 60 m T; (f) B = 90 m T.

occurred and irregular humps were observed on the rear of keyhole wall, due to unstable pressure balance on the keyhole wall. Additionally, the spray transferring mode under these welding parameters was observed. The droplet was generated at the tip of the wire and then grew to a certain size at t_0+3.0 ms. The droplet was detached from the end of the wire at t_0+4.0 ms. At t_0+7.0 ms, the droplet dropped into the rear of the keyhole and severe humps of keyhole wall were produced, which was consistent with the study of (Huang et al., 2020). Moreover, the impacted force of the droplet on the molten pool also aggravated the fluctuation of keyhole. When 20 m T of lower magnetic flux density was employed, the droplet transition was more unstable while the mode and cycle of droplet transition was similar with that without external magnetic field. Besides, the fluctuation of keyhole was also not improved and a series of humps were generated on the wall of keyhole. However, when magnetic flux density was increased to 90 m T, the significantly different behavior of droplet transition and keyhole fluctuation from that under NMFD was observed. The swigged droplet was observed and the direction of droplet transition was changeable during droplet transferring process from t_0+2.0 ms to t_0+4.0 ms. In this case, the droplet detached from the tip of the wire transferred into the molten pool away from the keyhole under the effect of external magnetic field force. Moreover, almost smooth keyhole wall and few bulges were detected, which implied that the high magnetic flux density had an important influence on the stabilization of the keyhole during the laser-MIG hybrid welding.

The difference of droplet transition behaviors between with and without external magnetic field could be explained by the forces of droplet. In the droplet transition process during laser-MIG hybrid welding, (Chen et al., 2018) and (Liu et al., 2018) have suggested that the forces acting on the droplet mainly consisted of gravity (***Fg***), self-induced electromagnetic force (***Fse***), surface tension (***Fst***), plasma flow force (***Fp***), and metal vapor jet force (***Fv***). Above forces could be calculated by Eqs. (4–8).

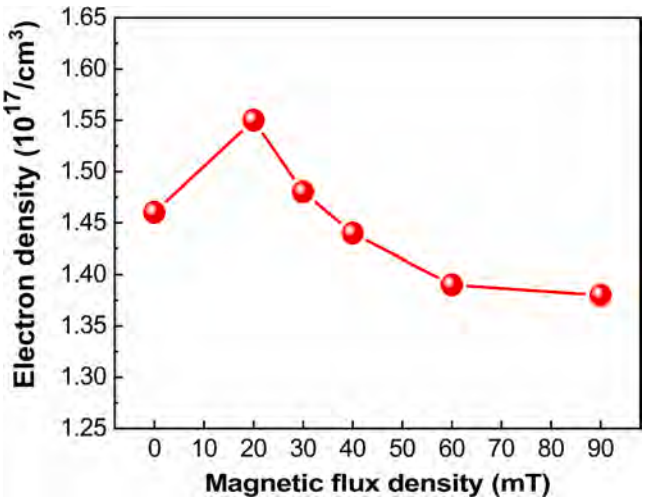

Fig. 9. Average electron density versus magnetic flux density.

The gravity force ***Fg*** could be calculated as

$$\boldsymbol{Fg} = \frac{4}{3}\pi r_d^3 \rho g \tag{4}$$

Where, r_d was the radius of droplet, ρ was the density of droplet, g was the gravitational acceleration.

The self-induced electromagnetic force ***Fse*** could be considered as

$$\boldsymbol{Fse} = \frac{\mu_0 I^2}{4\pi}\left\{ln\frac{r_d sin\theta}{r_w} - \frac{1}{4} - \frac{1}{1-cos\theta} + \frac{2}{(1-cos\theta)^2} ln\frac{2}{1+cos\theta}\right\} \tag{5}$$

Where, I was the welding current, r_w was the radius of filler wire, respectively. θ was the maximum angle between the electrode axis and point at which arc contacted droplet.

The surface tension force ***Fst*** could be obtained as

$$\boldsymbol{Fst} = 2\pi r_w \gamma \tag{6}$$

Where, γ was the surface tension.

The plasma flow force ***Fp*** could be calculated as

$$\boldsymbol{Fp} = \frac{1}{2} C_{ds} \rho_g v_g^2 \pi r_d^2 \left(1 - \frac{r_w^2}{2r_d^2}\right) \tag{7}$$

Where, ρ_g was the gas density, v_g was the gas velocity.

The metal vapor jet force ***Fv*** was considered as

$$\boldsymbol{Fv} = \begin{cases} \frac{1}{4\pi R_h^2} C_D A \rho_m^2 V_0^2 \left(\frac{N_\alpha K_\beta T_s^{\frac{3}{2}}}{M_\alpha B_0}\right) exp\left(-\frac{U}{T_s}\right) exp\left(-\frac{D_{LA}^2}{2R_h^2}\right), & D_{LA} \le R_h \\ 0, & D_{LA} > R_h \end{cases} \tag{8}$$

Where, R_h was the metal vapor distribution parameters, C_D was the aerodynamic drag coefficient, A was plasma acting area, p_m was the density of plasma, V_0 was a constant (3.4 × 102 ms − 1), N_α was Avogadro's constant, K_β was Boltzmann constant and T_s was the surface temperature of melted zone.

During the laser-MIG hybrid welding, as stated by the analysis of (Zhu et al., 2020), the droplet was driven by the resultant forces (***Fr***) away from the tip of wore towards molten pool. When droplet remained on the wire:

Fr=Fg+Fse+Fst+Fp+Fv

When droplet was detached from the wire:

Fr=Fg+Fse+Fp+Fv

Among these forces, the ***Fg***, ***Fse*** and ***Fp*** were the forces that promoted the droplet transition toward molten pool while the ***Fst*** and ***Fv*** were impeded forces. Therefore, the droplet was driven toward keyhole under the effect of the resultant force of these forces as shown in Fig. 12 (a). However, when external magnetic field was employed, the arc plasma was more compressed in the transverse direction than that without an external magnetic field, leading to larger direction angle of the plasma flow force (***Fp***) with the wire axis. In this case, the direction of the resultant force of droplet was biased toward behind the keyhole. Besides, the ampere force generated by the interaction of current in droplet and external magnetic field played an important role in droplet transition. As analyzed by (Zhu et al., 2020), a torques which pushed the droplet to slip around current centerline was obtained under external alternating magnetic field. When droplet was spinning under the ampere force, the centrifugal force ***Fc*** had to be considered in Eq. (9),

$$\boldsymbol{Fc} = mw^2 r \tag{9}$$

Where, m was mass of droplet, w was angular speed of droplet and r was radius of droplet.

With the increase of magnetic flux density, the centrifugal force and effective potential energy of spinning droplet was increased. Therefore, the resultant force (***Fr***) of droplet under external magnetic field was inclined to be downward, which was also beneficial for droplet transition toward the molten pool behind the keyhole instead of dropping into the location of keyhole.

Besides, it was noted that the impacted force of the droplet on the molten pool also could aggravate the fluctuation of keyhole. When the droplet was transferred to molten pool behind the keyhole with HMFD instead of dropping into the keyhole, which was also beneficial for stabilization of keyhole. Additionally, (Üstündağ et al., 2021) and (Xu et al., 2019) had proposed that the Lorentz force produced by the interaction of external magnetic flux density and melt flowing could reduce the melt displacement within molten pool and increase the homogeneity of the heat distribution in the thickness direction, leading to stabilization of keyhole. However, the detailed influencing mechanism of external magnetic field on stabilization of keyhole still needed further study.

3.3. Penetration mechanism of hybrid heat source to welded plate

In this study, the different weld depths were obtained with the same laser-MIG hybrid welding parameters under different external magnetic flux density. In accordance with the influence of alternating magnetic field on weld depths, the interaction of laser attenuation and hybrid plasmas, droplet transitions and keyhole behaviors under varying magnetic flux density was presented. The influencing factors of penetration ability of hybrid heat source to welded plate were depicted in Fig. 13.

The primary factor was the laser-induced plasma at the channel of laser beam. Alternating magnetic field could compress the shape of arc and disperse laser-induced plasma. In this case, more compressed arc was beneficial for erupting along the channel of laser beam under LMFD, leading to higher attenuation of laser energy. Besides, weaker shielding effect of laser-induced plasma on laser power was obtained due to the dispersed effect of HMFD on laser-induced plasma. As shown in Fig.12 (b), the second factor which should be considered was absorption and reflection of laser energy by droplet. When droplet was transferred toward the front of keyhole, the droplet would be broken and part of droplet would be gradually evaporated. In this process, the part of laser energy would be absorbed and reflected by the droplet. However, alternating magnetic field changed the force condition of droplet and promoted droplet of smaller size to drop into the molten pool behind the

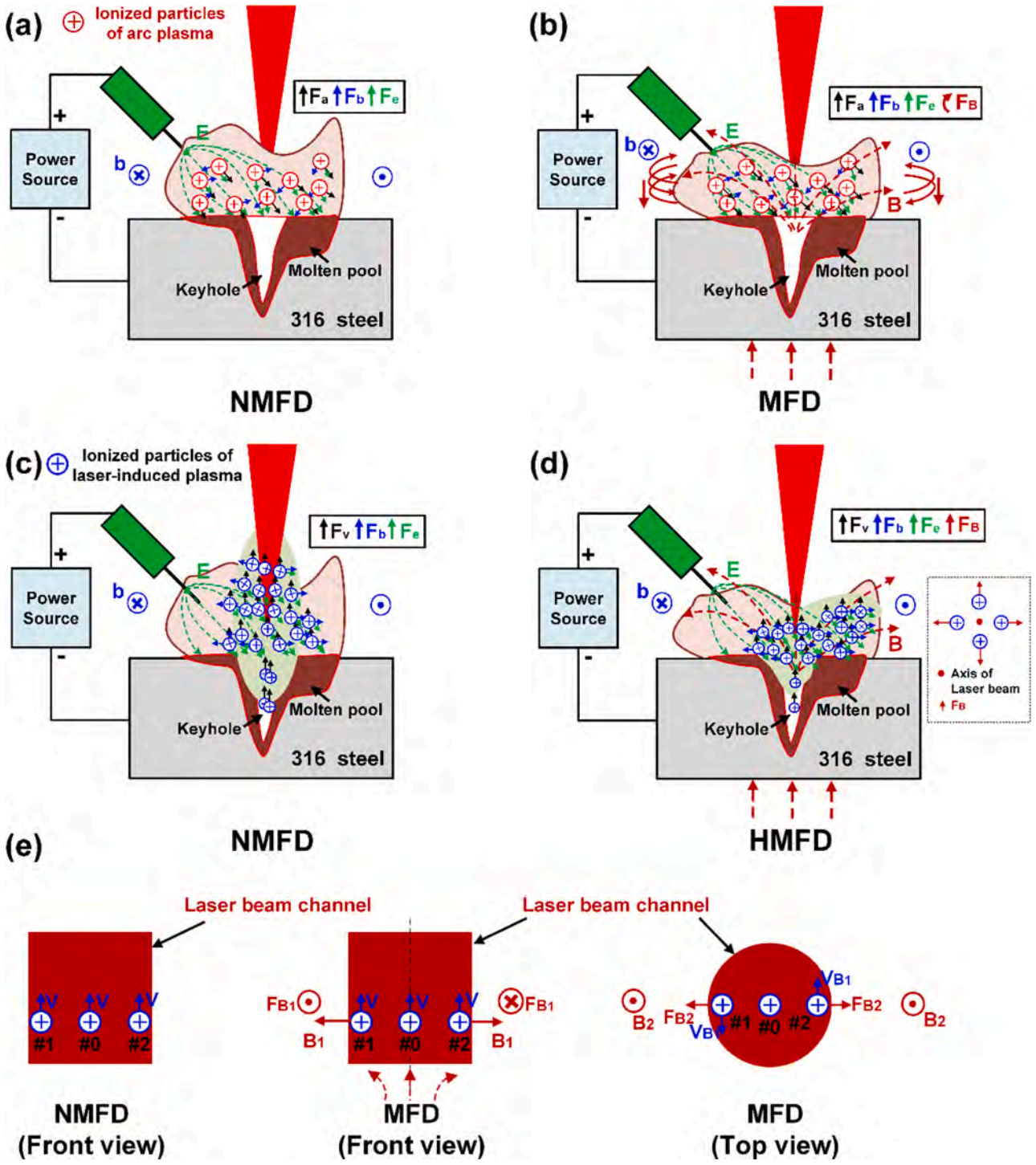

Fig. 10. Motion mechanism of ionized particles of arc plasma and laser-induced plasma during laser-MIG hybrid welding with and without alternating magnetic field: (a) ionized particles of arc plasma without alternating magnetic field; (b) ionized particles of arc plasma with alternating magnetic field; (c) ionized particles of laser-induced plasma without alternating magnetic field; (d) ionized particles of laser-induced plasma with higher magnetic flux density; (e) analysis of dispersing effect of magnetic field on laser-induced plasma.

keyhole, which increased the laser energy that was used to penetrate weld plate. Finally, the stabilization of keyhole helped the laser beam to penetrate deeper depth of base metal instead of employing laser energy to eliminate the hump of keyhole wall. The position and size of the droplet dropping into the molten pool was changed by external magnetic field, which decreased the impact force of the droplet on the keyhole and improved the stabilization of keyhole. It was also a factor that depth of laser-MIG hybrid welds was increased by the external magnetic field. Moreover, it must be admitted that laser-MIG hybrid welding was a complex process including plasma plume, droplet transition, keyhole fluctuation and molten pool behaviors. The behaviors of keyhole inside the molten pool under external magnetic field should be taken into account in the further study.

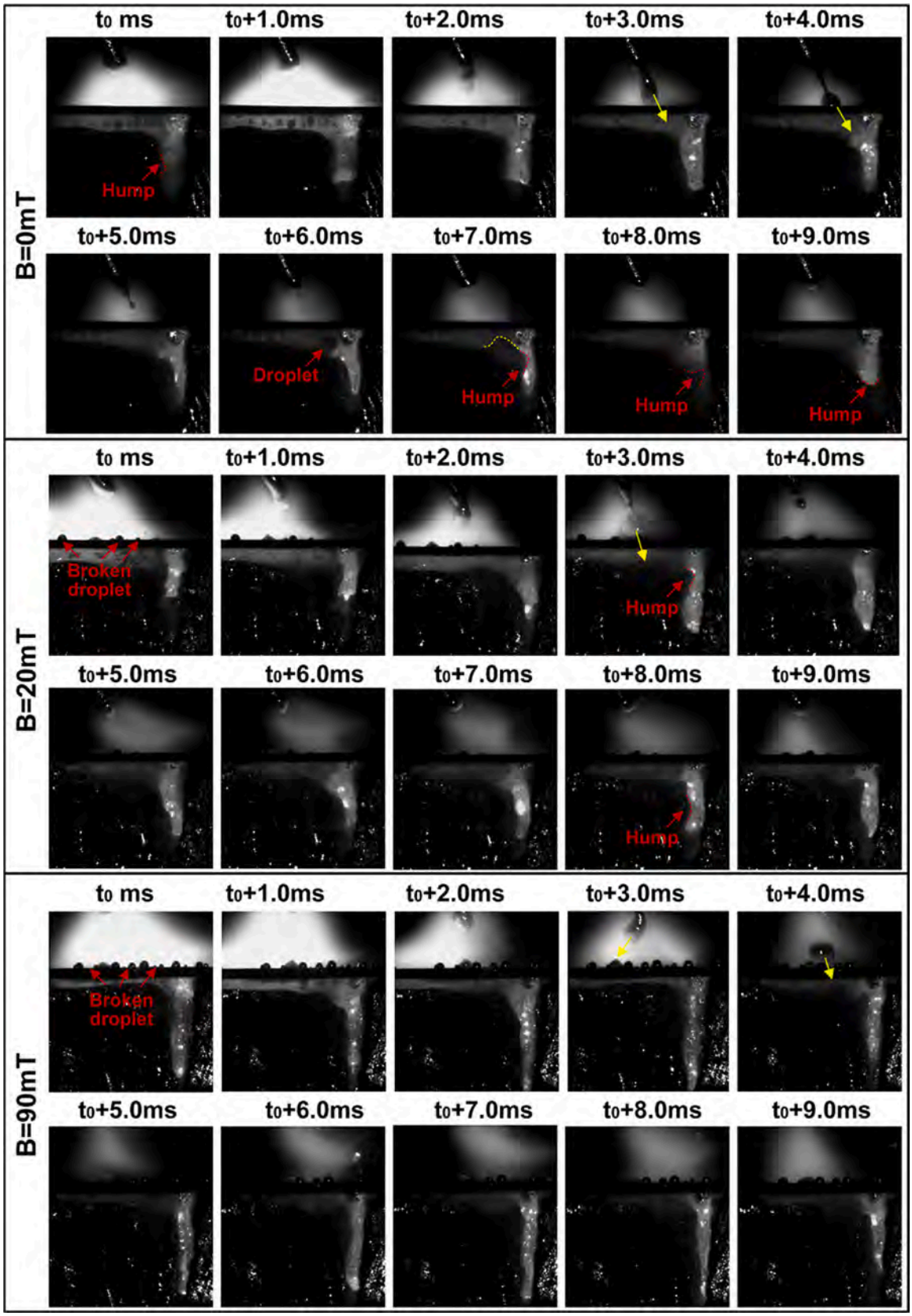

Fig. 11. Dynamic behavior of the keyhole and the droplet transition during laser-MIG hybrid welding. when B = 0 m T, B = 20 m T and B = 90 m T.

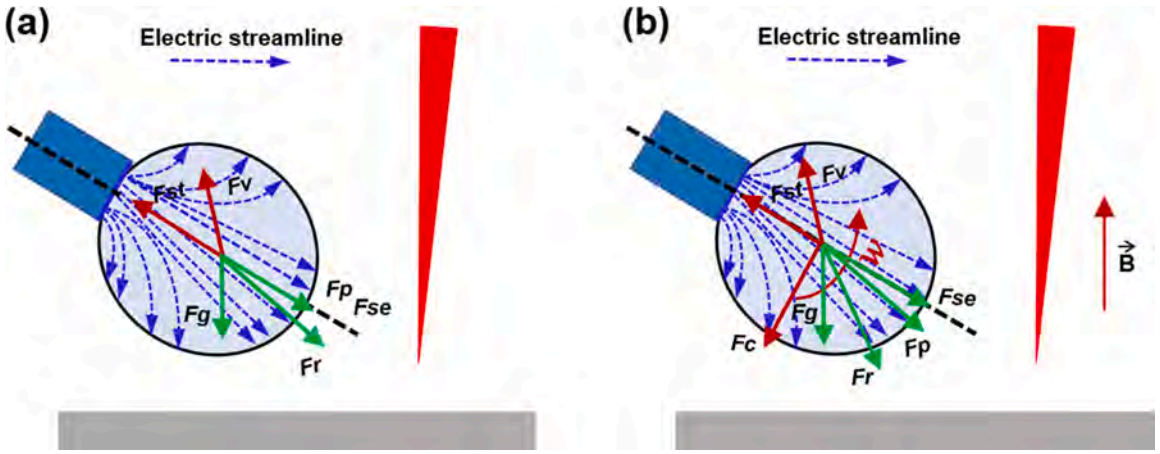

Fig. 12. Schematic of force analysis on droplet without and with magnetic field: (a) without magnetic field; (b) with magnetic field.

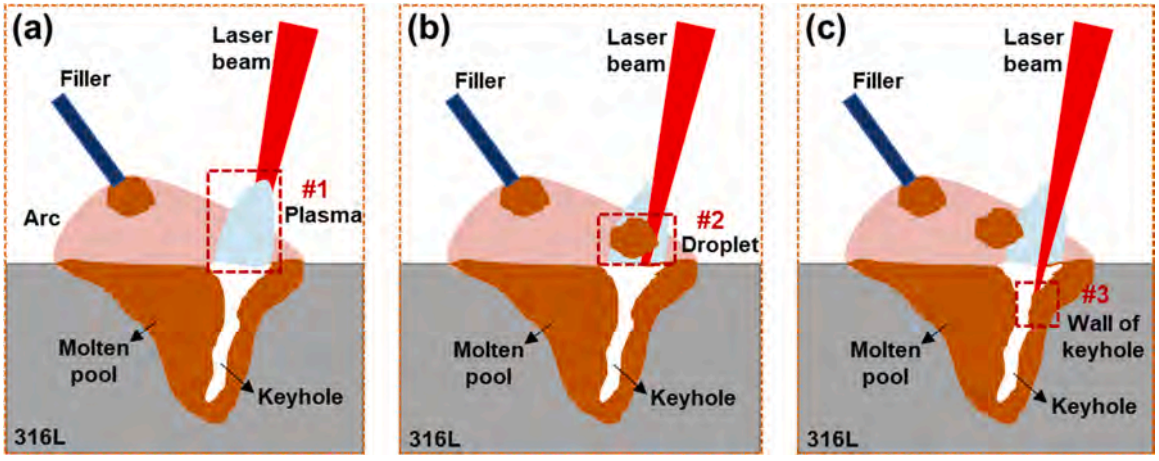

Fig. 13. Schematic of the factors influencing penetration ability of laser beam to welded plate:
(a) factor #1: welding plasma; (b) factor #2: droplet; (c) factor #3: wall of keyhole.

4. Conclusions

The following conclusions were obtained from the above results and discussion about change of penetration depth of 316 stainless steel laser-MIG hybrid welded joint under different magnetic flux density.

(1) Obvious differences on weld depth was observed in the laser-MIG hybrid welded joint under different magnetic flux density. The weld depth (3.14 ± 0.08 mm) and depth to width (0.503 ± 0.008) under LMFD with 20 m T was smaller than that (4.08 ± 0.06 mm and 0.709 ± 0.005) without an external magnetic field while the weld depth (4.35 ± 0.09 mm) and depth to width (0.70 ± 0.006) under HMFD with 90 m T was greater compared to that under B = 0 m T.

(2) The shape of arc plasma was more compressed when alternating magnetic field was employed due to the effect of Lorentz force exerted by external magnetic field, which resulted in more volume of laser-induced plasmas at the channel of laser beam under LMFD (B = 20 m T and B = 30 m T). However, the laser-induced plasmas were dispersed away from the channel of the laser beam when stronger Lorentz force was generated by HMFD (B = 60 m T and B = 90 m T), leading to weaker shielding effect on laser energy.

(3) The alternating magnetic field had a significant influence on forces condition and transition path of droplet. The droplet was transferred into the molten pool behind the keyhole under the effect of external magnetic field force instead of dropping into location of the keyhole, which also decreased attenuation of laser energy.

(4) The hump of keyhole wall was obviously decreased and more stable keyhole was obtained when magnetic flux density was 90 m T, due to decreased impact force of droplet on the keyhole. It also helped the laser beam to penetrate deeper depth of base metal.

Author statement

Fuyun Liu: Data curation, Writing - original draft. **Bingxiao Xu**: Investigation. **Kuijing Song**: Methodology, Writing - review & editing. **Caiwang Tan**: Conceptualization, Methodology, Writing - review & editing. **Hongyun Zhao**: Supervision. **Guodong Wang**: Validation. **Bo Chen**: Writing - review & editing. **Xiaoguo Song**: Writing - review & editing.

Declaration of Competing Interest

The authors declare that they have no known competing financial interests or personal relationships that could have appeared to influence the work reported in this paper.

Acknowledgments

The research was supported by National Natural Science Foundation of China (Grant No. 52074097) & (Grant No. 51875129).

References

Bachmann, M., Avilov, V., Gumenyuk, A., Rethmeier, M., 2016. Numerical assessment and experimental verification of the influence of the Hartmann effect in laser beam welding processes by steady magnetic fields. Int. J. Therm. Sci. 101, 24–34.

Bagger, C., Olsen, F.O., 2005. Review of laser hybrid welding. Journal of Laser Applications 17, 2–14.

Chen, M., Li, X., Liu, L., 2012. Effect of electric field on interaction between laser and arc plasma in laser–Arc hybrid welding. Ieee Trans. Plasma Sci. 40, 2045–2050.

Chen, X., Yu, G., He, X., Li, S., Miao, H., 2018. Effect of droplet impact on molten pool dynamics in hybrid laser-MIG welding of aluminum alloy. Int. J. Adv. Manuf. Technol. 96, 209–222.

Chen, X., Mu, Z., Hu, R., Liang, L., Murphy, A.B., Pang, S., 2019. A unified model for coupling mesoscopic dynamics of keyhole, metal vapor, arc plasma, and weld pool in laser-arc hybrid welding. J. Manuf. Process. 41, 119–134.

Chiang, S., Aibright, C.E., 1992. CO2 laser beam - materials iteractions in the welding of mild steel. Part 2: effects of plume suppression on heat transfer efficiencies in argon shielded laser beam welding. ICALEO, 491522.

Dilthey, U., Wieschemann, A., 1999. Prospects by Combining and Coupling Laser Beam and Arc Welding Processes. International Institute of Welding. IIW Doc. XII-1565-99.

Gao, M., Chen, C., Hu, M., Guo, L., Wang, Z., Zeng, X., 2015. Characteristics of plasma plume in fiber laser welding of aluminum alloy. Appl. Surf. Sci. 326, 181–186.

Huang, S., Yang, X., Chen, H., Cai, C., Xu, L., 2020. Effect of droplet transfer on pore formation in laser-pulsed metal inert gas hybrid welding of A7N01P aluminum alloy. J. Laser Appl. 32, 012011.

Katayama, S., Yohei, A., Mizutani, M., Kawahito, Y., 2011. Development of deep penetration welding technology with high brightness laser under vacuum. Phys. Procedia 12, 75–80.

Kawahito, Y., Kinoshita, K., Matsumoto, N., Katayama, S., 2009. Visualization of refraction and attenuation of near-infrared laser beam due to laser-induced plume. J. Laser Appl. 21, 96–101.

Lacroix, D., Jeandel, G., Boudot, C., 1997. Spectroscopic characterization of laser-induced plasma created during welding with a pulsed Nd:YAG laser. J. Appl. Phys. 81, 6599–6606.

Li, M., Xu, J., Huang, Y., Rong, Y., 2018. Improving keyhole stability by external magnetic field in full penetration laser welding. JOM 70, 1–6.

Liu, S., Chen, S., Wang, Q., Li, Y., Zhang, H., Ding, H., 2017. Analysis of plasma characteristics and conductive mechanism of laser assisted pulsed arc welding. Opt. Lasers Eng. 92, 39–47.

Liu, S., Zhang, F., Dong, S., Zhang, H., Liu, F., 2018. Characteristics analysis of droplet transfer in laser-MAG hybrid welding process. Int. J. Heat Mass Transf. 121, 805–811.

Luo, Y., Tang, X., Lu, F., Chen, Q., Cui, H., 2015. Effect of subatmospheric pressure on plasma plume in fiber laser welding. J. Mater. Process. Technol. 215, 219–224.

Shcheglov, Uspenskiy S.A., Gumenyuk, A.V., Petrovskiy, V.N., Rethmeier, M., M, Y.V, 2011. Plume attenuation of laser radiation during high power fiber laser welding. Laser Phys. Lett. 8, 475–480.

Steen William, M., 1980. Arc augmented laser processing of materials. J. Appl. Phys. 51, 5636–5641.

Tse, H.C., Man, H.C., Yue, T.M., 1999. Effect of magnetic field on plasma control during CO2 laser welding. Opt. Laser Technol. 31, 363–368.

Üstündağ, Ö., Bakir, N., Gumenyuk, A., Rethmeier, M., 2021. Influence of oscillating magnetic field on the keyhole stability in deep penetration laser beam welding. Opt. Laser Technol. 135, 106715.

Wang, C.M., Meng, X.X., Huang, W., Hu, X.Y., Duan, A.Q., 2011. Role of side assisting gas on plasma and energy transmission during CO2 laser welding. J. Mater. Process. Technol. 211, 668–674.

Wang, J., Sun, Q., Feng, J., Wang, S., Zhao, H., 2017. Characteristics of welding and arc pressure in TIG narrow gap welding using novel magnetic arc oscillation. Int. J. Adv. Manuf. Technol. 90, 413–420.

Xu, J., Rong, Y., Huang, Y., 2019. Magnetic-field-Induced partial-to-Full penetration evolution and its mechanism during laser welding. JOM 71, 2296–2302.

Zhu, Z., Ma, X., Wang, C., Mi, G., 2020. Modification of droplet morphology and arc oscillation by magnetic field in laser-MIG. Hybrid welding. Opt. Lasers Eng. 131, 106138.

Zuo, T., Dorko, E.A., Xiao, R., Moler, J.L., Volz, R., 1998. Experimental Research on the Influence of Laser-induced Plasma on Beam Focusing During High-power CO 2 Laser Materials Processing, 3268, p. 62.